Hindawi
Scientific Programming
Volume 2021, Article ID 3554718, 10 pages
https://doi.org/10.1155/2021/3554718

Research Article

Optimized Backprojection Filtration Algorithm for Postoperative Reduction and Analysis of Respiratory Infection-Related Factors of Pelvic Fractures by CT Imaging

Aihua Pu,[1] **Hua Wang**,[2] **and Jichong Ying**[3]

[1]*Department of Pneumology, Ningbo No.6 Hospital, Ningbo 315040, Zhejiang, China*
[2]*Department of Radiology, Ningbo No.6 Hospital, Ningbo 315040, Zhejiang, China*
[3]*Department of Orthopedics, Ningbo No.6 Hospital, Ningbo 315040, Zhejiang, China*

Correspondence should be addressed to Aihua Pu; 3116320058@m.fafu.edu.cn

Received 28 August 2021; Accepted 20 October 2021; Published 8 November 2021

Academic Editor: Gustavo Ramirez

To explore the computed tomography (CT) imaging characteristics and BPF algorithm fine lung CT image efficiency for the diagnosis of pelvic fracture patients and assist clinicians to carry out the disease care and treatment, CT images based on optimized back-projection filtering (BPF) algorithm were utilized to diagnose postoperative reduction of pelvic fractures and penetrating lung infection caused by long-term bed rest. A total of 100 patients with pelvic fracture were selected and all of them underwent pelvic fracture surgery and were rolled into conventional CT diagnosis group (conventional group) and BPF algorithm optimized CT image diagnosis group (BPF group). One group used conventional CT images to guide pelvic reduction and detect lung infections, and the other used BPF algorithm to optimize the images. The results showed that the BPF group was superior to the conventional CT group in both image clarity and shadow area, and the peak signal-to-noise ratio (PSNR) was significantly better than that of the conventional group ($P < 0.05$). Nine more cases were detected in the algorithm group than in the conventional group, and the incidence of complications was 48% in the conventional group and 28% in the BPF group, with a statistical difference of 20% between the two groups ($P < 0.05$). In addition, the satisfaction of returning patients was 96% in the BPF group and 77% in the conventional group ($P < 0.05$). The diagnosis of pulmonary infection was more obvious in the BPF group, indicating that BPF optimization of the CT image was suitable for clinical diagnosis and had a practical application value.

1. Introduction

The pelvis is composed of skeleton and coccyx, and two skeletons are formed by fusion of ilium bone, ischium, and pubic bone, which is an important part connecting human bones and joints [1]. Pelvic is the anterior ring of the pelvis and the skeleton of the back of the skull. Pelvic fractures refer to joint dislocations, damage to the skeletal joint ligaments of the skeleton, and wing and bone fractures behind the fracture line [2]. In recent years, from the knowledge of pelvic fractures, pelvic anatomy, and biomechanics, traffic accidents, falls, and natural disasters accounts for 13% of all fractures, with a prevalence rate of 50–60% and a mortality rate of 10–25%. Image processing techniques and devices are constantly improved, which will further improve the humanization of the treatment of unstable pelvic fracture types and greatly reduce the mortality and incidence rate [3]. In recent years, with the continuous development of technology and medical instruments, the treatment of pelvic fractures has become more and more progressive and personalized.

CT imaging is the best diagnostic combination method for the treatment of pelvic fractures [4]. Treatment varies according to the type of fracture, and the incidence of pelvic open infection is about 15% [5]. Studies showed that the incidence of open infection in the treatment of posterior pelvic wheel injuries due to posterior infection is as high as 18 to 27 percent. Postoperative infection of pelvic fractures is not uncommon, most of which occur after open pelvic fractures [6]. However, surgical site infection after pelvic fracture is rare, and the risk

factors associated with infection have not been well reported. For patients who are bedridden because of a pelvic fracture, confusion, congestion, and edema appear at the bottom of the lungs due to heart failure and low immunity. Infection by bacteria and other pathogens causes severe pneumonia, with cough, fever, and phlegm as the main symptoms. Pulmonary infections can lead to serious complications if they are not well controlled, especially, in elderly patients with breathing difficulties, sepsis, and heart disease. Patients who are bedridden for a long time need not only treatment for major diseases and anti-infection treatment but also regular back massage to maintain movement and lung function [7]. The increase of neutrophils, positive sputum culture, and other examination results in patients with pneumonia can be used as the diagnostic benchmark for this disease [8]. However, due to the lack of specificity, clinical symptoms and chest CT symptoms must be combined to determine the patient's status. It is necessary to detect postoperative infection factors related to closed pelvic fractures and study the diagnosis and treatment of postoperative infection of pelvic fractures, thus providing clinical guidance on the diagnosis and treatment of postoperative infection of pelvic fractures.

CT is a new kind of science and technology which combines the most advanced technologies in radiology, informatics, microelectronics, and computer science. In 2004, a team led by Professor Xiaochuan Pan of the University of Chicago proposed an accurate CT reconstruction algorithm based on back-projection filtering [9]. This algorithm can accurately reconstruct the cross-sectional image of an object using the minimum projection data. BPF reconstruction algorithm is based on PI line reconstruction algorithm. The most important contribution of the BPF algorithm is solving the problem of accurate CT reconstruction by truncating the projection data along the horizontal direction of the detector. Therefore, the BPF algorithm is used to design the imaging strategy of the target region of interest (ROI) [10]. Moreover, it can reduce imaging scan, reconstruction time, and radioactivity. Although CT has been developed for many years and the hardware has been greatly improved, the classical filter back-projection algorithm has not been applied to the analysis of fracture surgery and pulmonary infection images in reconstruction algorithms.

Therefore, the BPF algorithm was studied, optimized, and applied in practice. The image refinement enhancement method based on BPF was used to reduce postoperative complications and pulmonary infection. Moreover, medical CT images were observed to detect the peak signal-to-noise ratio (PSNR) to determine the efficiency of noise reduction, and the imaging characteristics of pelvic recovery and pulmonary infection were studied. The BPF algorithm can be used to detect medical CT images, which can provide a theoretical basis for the application of CT images in the diagnosis of pelvic fracture reduction and subtraction pneumonia and provide practical needs for CT image diagnosis of other diseases.

2. Methods

2.1. Research Objects. A total of 100 patients with pelvic fractures admitted to the hospital from January 2018 to January 2021 were selected. All patients, with an average age of 45 years, underwent surgery for pelvic fractures, including men between 20 and 70 years of age. All patients were rolled into the conventional group (conventional CT diagnosis) and the BPF group (BPF algorithm was employed to optimize CT image diagnosis).

Inclusion criteria: (i) patients agreed to participate in the study and signed the written informed consent; (ii) patients who can adapt the surgery; (iii) patients who can adapt to anterior fixation for pelvic fractures; (iv) patients without surgical contraindications; (v) patients with closed pelvic fracture; (vi) open reduction and internal fixation were performed; (vii) patients had complete medical data and were followed up for more than one year.

Patients meeting any of the following exclusion criteria were excluded from the study: (i) patients with an autoimmune disease; (ii) patients with open pelvic fracture; (iii) those who withdrew due to other factors or did not complete the follow-up.

In this study, a total of 100 patients with pelvic fractures met the above inclusion criteria and exclusion criteria. This study had been approved by the Medical Ethics Committee of the hospital, and the families of the patients included in the study had all signed informed consent.

2.2. CT Examination. The patient's physiology was observed before the scan, venous access was established for shock correction, and the patient was transported to the CT room when conditions permitted. In the previous plate scan, the patients were scanned from the upper part of the pelvis to large or partial nodules and from the upper part of the cranial enteritis to the head and legs at 140 kV tube voltage, 350 mAs tube current, 0.55 s time, and 1.3 mm interval. The spacing was 5 mm, the detector in 256 columns was combined 40–50 cm, and the matrix was 512x512. CT scan data were transmitted and CT cross section data reconstruction in scan field was stored. The format was Digital Imaging and Communication in Medicine (DICOM) 3.0, and the data in the CT room burned CD for export.

2.3. BPF Algorithm Based on Spiral Scanning. It is assumed that the image function $f(x, y, z)$ is limited to a cylinder with a radius of d, and the height is $z.r$. The center axis is placed on the side of the z-axis as a b space vector, or it is written as $b = (X, Y, Z)$, so the scan trajectory is as follows:

$$\begin{aligned} &f(x, y, z) = 0, \\ &x2 + y2 > d2, \quad z < -zs. \end{aligned} \tag{1}$$

It is assumed that the trajectory meets two conditions that the scanning trajectory does not intersect the supporting cylinder, which means that the trajectory will not intersect the real image object, and is continuous and differentiable to the path, which is general and can satisfy many different scanning trajectories. In the 3D scanning trajectory, first, we define the ray source as follows:

$$\begin{aligned} B &= [s(p)] \\ &= [R(P)\cos P, R(p)\sin p, Z(P)], \end{aligned} \tag{2}$$

where p represents the angle of rotation and $s(p)$ is the path length with respect to the angle of rotation:

$$\begin{aligned} s(p) &= \int_0^p \left|\frac{\mathrm{d}b(p)}{\mathrm{d}p}\right| \mathrm{d}p, \\ D\left(\left(\vec{B}_0 S\right), \beta\right) &= \int_0^\infty \mathrm{d}t f\left(\vec{B}_0(S) + t\beta\right), \end{aligned} \tag{3}$$

where β is the direction vector of the X-ray passing through the point in the projection direction, which is expressed as follows:

$$\beta = \frac{\vec{B} - \vec{B}_0(p)}{\left|\vec{B} - \vec{B}_0(p)\right|}. \tag{4}$$

In three-dimensional scanning, $\vec{B} - \vec{B}_0(p)$ is projection data. Therefore, the BPF reconstruction algorithm based on the proportional unit and integral unit (PI) line theory is given as the equations as follows, and the content of the equation includes the entire reconstruction step [11]:

$$\begin{aligned} f_c(y_c, s_a, s_b) = {} & \frac{1}{2\pi^2} \frac{1}{\sqrt{(y_{c2} - y_c)(y_c - y_{c1})}} \left\{ \int_{y_{c1}}^{y_{c_c}} \frac{\mathrm{d}y_c}{y_c - y_c'} \sqrt{(y_{c2} - y_c')(y_c' - y_{c1})} \right\} y \\ & \int_{2_a'} \left|\vec{r}(y_c') - \vec{r}_0(s)\right|^2 \left\{ \begin{array}{l} \left[-\dfrac{\mathrm{d}\vec{r}_0(s)}{\mathrm{d}s} \cdot \beta \right] P(u_i, v_d, s) + A(u_d', v_d') \dfrac{\mathrm{d}\vec{r}_0(s)}{\mathrm{d}s} \\ \\ \left[\hat{e}_u(s) \dfrac{\partial}{\partial u_d'} + \hat{e}_v(s) \dfrac{\partial}{\partial v_d'} \right] P(u_d, v_d, s) \end{array} \right\} \\ & + \frac{C}{2} \left\{ \frac{\sqrt{(l - y_{c2})(l - y_{c1})}}{l - y_c} + \frac{\sqrt{(l + y_{c2})(l + y_{c1})}}{l + y_c} \right\}. \end{aligned} \tag{5}$$

In the above equation, each point is expressed as

$$\begin{aligned} u &= -\frac{w}{S(s)} u_d, \\ v &= -\frac{w}{S(s)} v_d. \end{aligned} \tag{6}$$

β meets the following condition:

$$\begin{aligned} \beta &= \frac{1}{A(u_d, v_d)} \left[u_d \hat{e}_u(s) + v_d \hat{e}_v(s) - S(s) \hat{e}_w(s) \right], \\ A(u_d, v_d) &= \sqrt{u_d^2 + v_d^2 + S^2(s)}. \end{aligned} \tag{7}$$

According to the above equations, the algorithm implementation process is summarized, which has seven steps (Figure 1).

2.4. Image Quality Assessment. The rapid development of image processing technology has brought rapid development to the world, and reconstruction algorithms in this field are very rich. However, methods for objectively evaluating the advantages and disadvantages of correction, noise elimination, and reconstruction algorithms in the field of medical image processing are still areas of research that need improvement [12]. Therefore, the research of medical image quality evaluation algorithms is also one of the important contents of this profession. Objectively, image quality evaluation algorithms are divided into two categories. The emergence of structural similarity and information fidelity focuses on image feature extraction. In the field of objective evaluation of image quality, various image quality feature extraction algorithms have appeared one after another. Through research in the field of human vision system (HVS), the visual characteristics of human eyes are understood [13]. The research so far includes channel characteristics, contrast sensitivity, masking effect, and visual nonlinearity. Specifically, the simplified model of HVS is presented as Figure 2.

To evaluate the algorithm as objectively as possible, the parameter evaluation used in the image quality evaluation algorithm, namely, the PSNR, was used to evaluate the size of the image noise. Since it was the doctors who recognized the medical images of patients' diseases, HVS must be considered to evaluate fairly and accurately. In this way, the evaluation result was close to the human visual effect.

2.5. Peak Signal-to-Noise Ratio. The traditional methods of flat image quality evaluation are divided into subjective and objective aspects. The main method of subjective evaluation is selecting a group of observers to analyze and determine the quality of the image and give scores [14]. This method is relatively credible, but its operation is reliable because of its complexity, long time, and many uncertain and unreliable

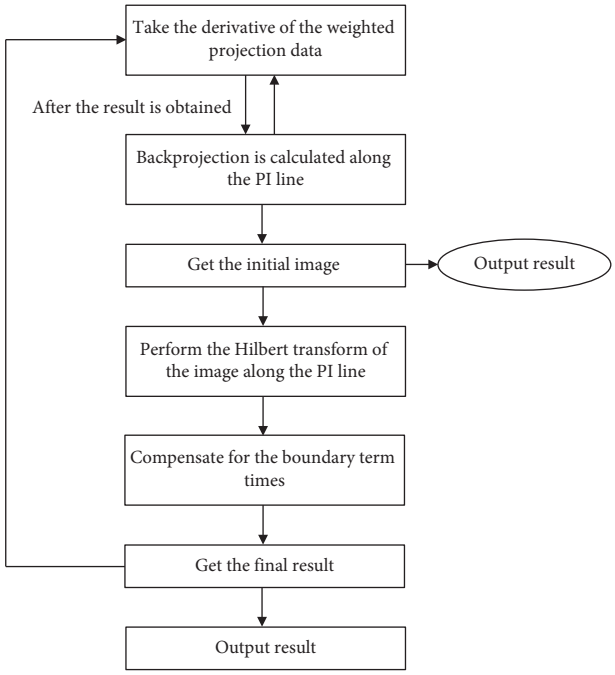

Figure 1: The process of BPF algorithm implementation.

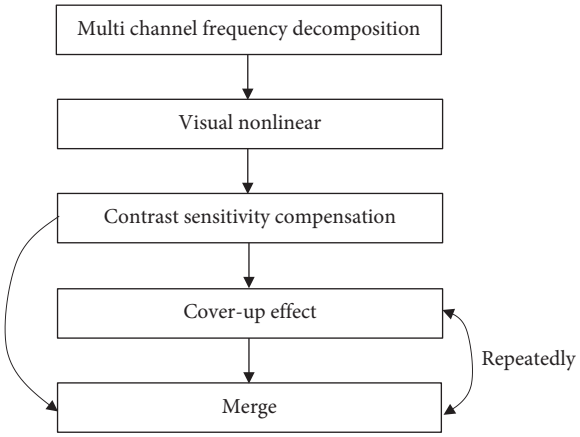

Figure 2: HVS evaluation of the simplified model.

factors. Objective evaluation methods have many advantages and are widely used, such as high-speed, low-cost, and embeddable digital image processing in the field of digital systems. PSNR is the most commonly used test standard:

$$\mathrm{MSE} = \frac{\sum_{w=0}^{M}\sum_{e=0}^{N}\left[\alpha(w,e)-\alpha_0(w,e)\right]^2}{\mathrm{MN}}. \tag{8}$$

Among them, MSE is the mean square error, and M and N are the length and width of the image, respectively. Therefore, the PSNR is as follows:

$$\mathrm{PSNR} = 10\lg\frac{\left(3^{\mu}-2\right)^2}{\mathrm{MSE}}. \tag{9}$$

3^{μ} is the square of the maximum possible signal value of the image, and μ is the number of pixel bits, so the larger the PSNR value, the better the image quality.

The algorithm calculates simply from the point of view of mathematical statistics. The digital image information is considered to be multiple isolated points. Therefore, the algorithm based on this statistical model ignores the correlation between adjacent pixels [15]. When the PSNR parameter is used to deal with unstructured distortion in a graph, the algorithm has a judgment ability consistent with human subjective cognition. From this point of view, PSNR is a good indicator for evaluating the degree of noise distortion.

2.6. Statistical Processing. Graphpad prism 5.0 was employed to carry out statistical processing to each data. The data were expressed as mean ± standard error using SPSS 20.0 to analyze the differences between groups. The t-test of independent samples was used to detect blood vessel diameter experiments and angiogenesis experiments. $P < 0.05$ was statistically different.

3. Results

3.1. Visual Comparison of Image Optimization Efficiency of Natural Optimization and BPF Algorithm Optimization. The PSNR evaluation effect was verified in Matlab, and the medical CT image plus noise was used for verification. The results were shown in Figures 3–5. In the CT images of the head and elbow, the original image contained some noise, and the skull edge was not clear. Conventional optimized CT images of the head and elbow improved the resolution slightly, but the image details were lost. The head and elbow CT images optimized by BPF algorithm had improved image clarity, reduced noise, and retained image details. In the original head MRI image, there were some artifacts in the image, but the BPF algorithm optimized the detail retention of the MRI image and had a better effect on removing artifacts.

For the image after addition of different degrees of noise, the axis represented the amount of noise added, and the unit was dby. The processed images were compared with the original ones. PSNR parameter evaluation test was performed. The x-axis represented the PSNR value, and the evaluation was shown in Figure 6.

From Figures 3–5, the edge information of the image was lost in the usual optimization processing, and the degree of image blur was large. The processing result of the BPF algorithm had a good visual effect, the image noise was effectively suppressed, and the edge details were maintained well. From the PSNR evaluation in Figure 6, as the noise decreased, the PSNR value increased accordingly. The PSNR parameter can linearly indicate the size of the noise in the image, and therefore, it is used in the field of image quality evaluation. The PSNR obtained by the BPF algorithm was better than the unprocessed image and ordinary optimization. Therefore, BPF algorithm optimization had strong optimization and edge detail protection capabilities.

3.2. Two Groups of Pelvic Fractures Combined with Pelvic Organ Damage. In the conventional group, 16 cases of

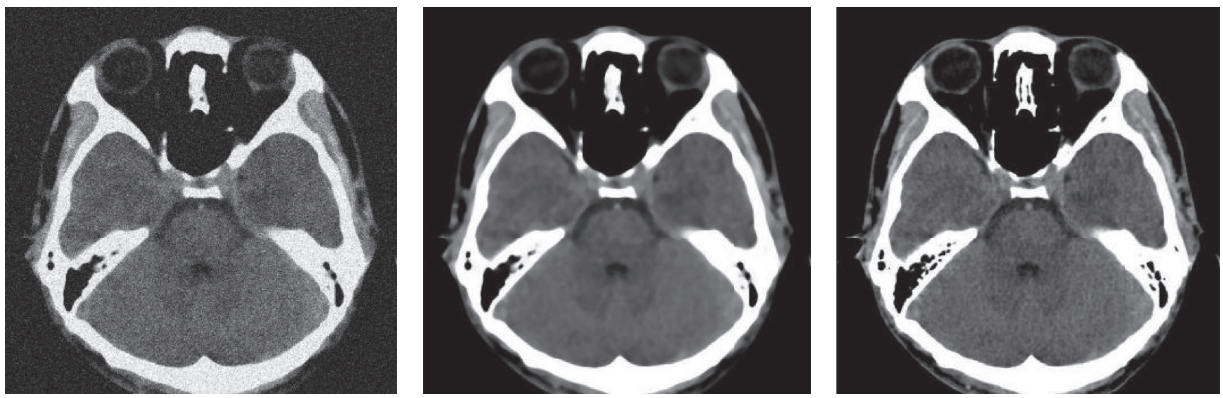

(a) (b) (c)

Figure 3: Visual comparison of head CT images optimized and processed in different ways. (a) original head CT image; (b) routine optimization of head CT image; (c) BPF algorithm optimization of head CT image.

(a) (b) (c)

Figure 4: Visual comparison of elbow CT images optimized and processed in different ways. (a) original elbow CT image; (b) routine optimization of elbow CT image; (c) BPF algorithm optimization of elbow CT image.

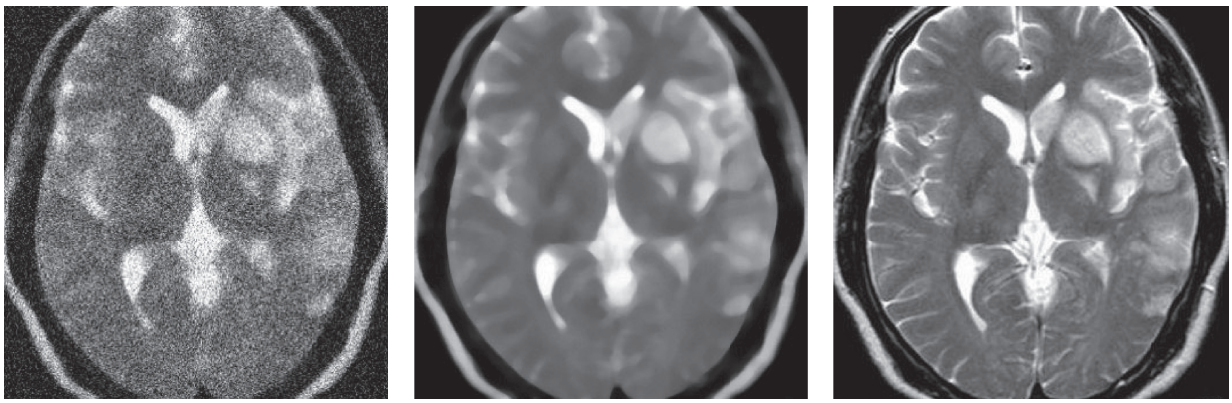

(a) (b) (c)

Figure 5: Visual comparison of head MRI images optimized and processed in different ways. (a) original head MRI image; (b) routine optimization of head MRI image; (c) BPF algorithm optimization of head MRI image.

pelvic fractures were detected by the CT scan, including 8 cases of bladder fracture, 6 cases of posterior urethral injury, and 5 cases of pelvic hematoma. According to the image data of BPF algorithm, 25 cases of bladder rupture were diagnosed. There were 10 cases of anterior bladder wall rupture, 11 cases of posterior urethra injury, and 8 cases of pelvic

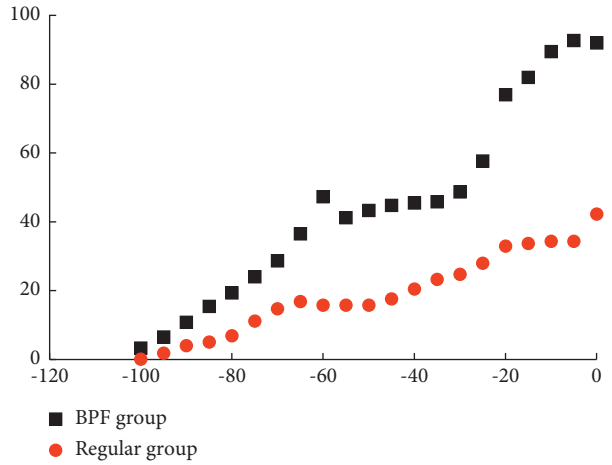

Figure 6: Two sets of PSNR evaluation.

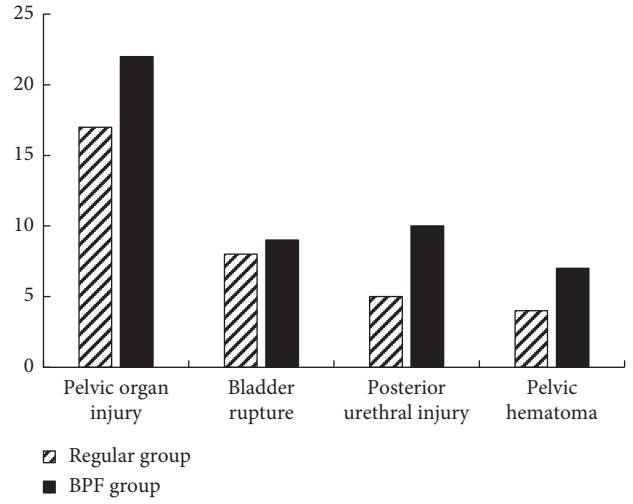

Figure 7: Comparison of the detection of pelvic fractures and pelvic organ damage between the two groups.

hematoma, indicating that the detection rate of complications of pelvic surgery in the BPF group was very high (Figure 7).

3.3. Comparison of the Incidence of Complications after Surgery between the Two Groups. The postoperative complications' statistics of the two groups were shown in Table 1. The postoperative complication rate of the first group was dramatically higher than that of the second group. There was a considerable difference between the two groups of data, which was statistically considerable ($P < 0.05$), indicating that the recovery was good and there were few complications after the BPF algorithm processing.

3.4. Evaluation of Curative Effect in Two Ways. After the efficacy evaluation, anatomical reduction was found in 42 cases in the conventional group, 45 cases were satisfactory, and 12 cases were unsatisfactory. In the BPF group, 59 cases were anatomically reduced, 56 cases were satisfactory, and 4 cases were unsatisfactory. Follow-up period ranged from 20 days to 8 months. According to the Matta criteria for efficacy evaluation [16], the clinical efficiency was excellent in 84 cases amd good in 39 cases, with an excellent and good rate of 95%. In the BPF group, 95 cases were excellent and 45 cases were good, with an excellent and good rate of 99%, as illustrated in Figures 8 and 9.

3.5. Visual Comparison of the Hypostatic Pneumonia Image Optimization Efficiency of the Natural Denoising Algorithm and the BPF Denoising Algorithm. The CT images of patients with hypostatic pneumonia were refined by the BPF algorithm, and the results are shown in Figure 10. CT image noise was dramatically reduced and lung shadow was clear, which was convenient for doctors to diagnose.

3.6. Comparison of Characteristics of Pulmonary Pneumonia and Infection between the Two Groups. Figure 11 showed the detection rate, unilateral, bilateral, and missed diagnosis rate of the conventional group and BPF algorithm group. Wedge-shaped consolidation was detected, and the shadow area was large. The density was

Table 1: Statistics of postoperative complications in the two groups.

	Physical movement disorders	Constipation	Nerve damage	Hypostatic pneumonia	Complication rate (%)
Conventional group	3	7	5	9	48
BPF group	2	6	1	5	28

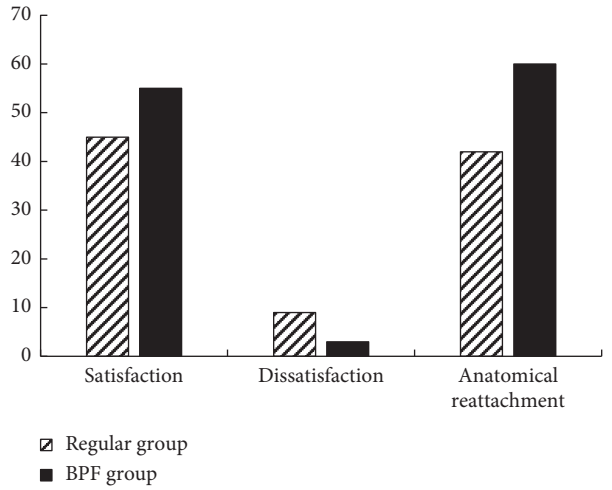

Figure 8: Comparison of patient satisfaction after treated with the two methods.

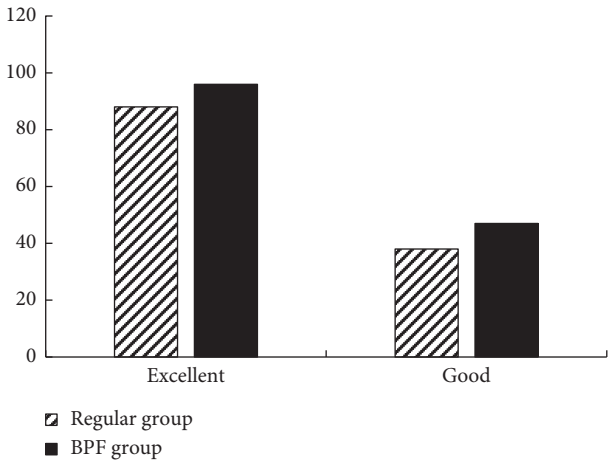

Figure 9: Comparison of the efficacy of the two methods.

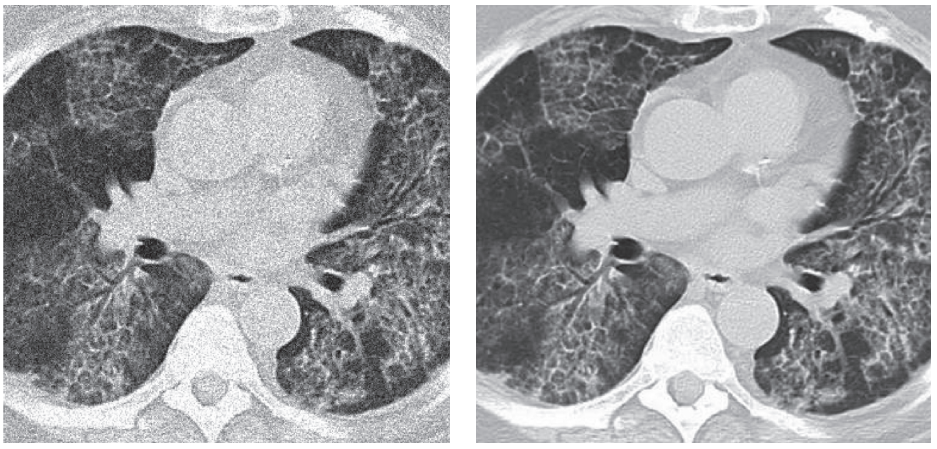

(a) (b)

Figure 10: Visual comparison diagram of CT images optimized in different ways. (a) original CT image of hypostatic pneumonia; (b) CT image of pendulous pneumonia processed by BPF algorithm.

increased, but the edge was blurred, suggesting a wide range of lesions and a more serious condition. The detection of large area of patchy shadow indicated that the lesion degree was inconsistent. The posterior medial to lateral displacement of the diaphragmatic angle was detected. There was a fluid density shadow in the chest wall, suggesting a pleural effusion. The uneven thickness of the soft tissue along the chest wall was detected by spotty, banded, or lumpy high-density shadow. Small adhesions were seen, suggesting pleural hypertrophy, calcification, or adhesions (Figure 12). In Figure 11, the detection rate of the BPF algorithm group was 86% and that of the conventional group was 64%, with a 22% difference between the two groups. The unilateral detection rate was 83% in the BPF group and 61% in the conventional group, with a 22% difference between the two groups. The bilateral detection rate was 92% in the BPF group and 71% in the conventional group, with a difference of 21% between the two groups. The BPF algorithm group missed detection rate was 4%, the conventional group missed detection rate was 30%, and the difference between the two groups was 26%. In Figure 12, it was found that the detection rate of the BPF algorithm group was better than that of the conventional group in wedge-shaped consolidation shadow, large-area patchy shadow, medial to lateral posterior diaphragm angle and banded soft tissue along the chest wall with uneven thickness.

4. Discussion

Pelvic fractures are a common type of fracture in surgery and treatment and are increasing every year. Fracture is common in the middle-aged elderly. If the patients do not receive timely and effective treatment and effective nursing, it will seriously threaten the life and health of patients. Patients with fracture will generally have negative emotions such as nervousness, restlessness, and depression, which will have a negative impact on the surgical treatment and prognosis of patients. In addition, postoperative side effects may increase postoperative pain and affect patient recovery and postoperative treatment. Therefore, to ensure the effect of surgical treatment and reduce the impact of complications, it is necessary to reduce the incidence of complications and ensure the recovery of patients [17].

Hypostatic pneumonia is a common complication in patients who are chronically bedridden. The specific diagnostic criteria of this disease are patients who are bedridden for a long time, cough, wheezing, dyspnea, fever, sepsis, poisoning and other systemic symptoms, and respiratory symptoms combined with angiography. Positive symptoms such as the lower lung field and the compressed shadow exudation of the lung field can basically be diagnosed as pendulous pneumonia. It is easy to diagnose the disease based on its history and clinical symptoms, but early detection and treatment are beneficial to the patient's prognosis. With the continuous development of imaging technology, X-ray and CT have gradually become common means for the diagnosis of chest diseases to continuously improve the brightness of imaging. CT helical scanning can avoid image overlap, and the three-dimensional structure of the lung is clearly displayed by multidimensional lung imaging, which is useful for finding tissue lesions. Relevant literature showed that CT scan not only has the current diagnostic value of lung diseases but also detects some risk factors, such as pulmonary edema, congestion, and exudation, which may cause pneumonia or worsen [18]. The patient population on chest examination was scattered with small irregularities and dense opacities according to the results of one or both lungs, indicating hydronema or pleural lesions. CT scan for low-dose pneumonia and pleural lesions can detect the nature and extent of the lesions.

Experimental results showed that the proposed model had good visual effects and good PSNR for natural image optimization. The edge details of the image were retained effectively, and the quality of CT image was obviously improved. The BPF group was superior to the conventional CT group in both image sharpness and shadow area, and the peak signal-to-noise ratio was significantly better than the conventional group ($P < 0.05$). Nine more cases were detected in the algorithm group than in the conventional group, and the complication rate was 48% in the conventional group and 28% in the BPF group, with a difference of 20% between the two groups. The detection rate of the BPF algorithm group was 86% and that of the conventional group was 64%, with a difference of 22% between the two groups ($P < 0.05$). The satisfaction of returning patients was 96% in the BPF group and 77% in the conventional group ($P < 0.05$). It was suitable for clinical diagnosis and had a practical application value. BPF algorithm was used to optimize CT images, which presented the most intuitive and comprehensive images of pelvic fractures and pelvic organ injuries. Chan et al. [19] proposed the CNN model based on level set contour constraint, which can realize the segmentation of bladder cancer from CT urography data. Useful information can be retained and the optimization efficiency of deep network can be improved by using the contour features of the level set to constrain the loss function of CNN. This is similar to the study in this work. Warner et al. [20] proposed a high-level implicit shared feature representation method based on deep learning. Boltzmann mechanism was used to build a deep network to find potential hierarchical features in three-dimensional block space. Then, multimodal DBM was used to extract joint feature representations from MRI and PET to further improve the accuracy of Alzheimer's disease focal regions. It was of high clinical value to confirm and clarify the classification of pelvic fracture, the choice of treatment plan, and the operation method and provide correct guidance for making detailed operation plan. Moreover, it was an important method to show the pulmonary infection caused by pelvic fracture and pelvic organ injury, and it played an important role in the prognosis of patients, which has high value in the imaging examination of pelvic fracture and pelvic organ injury. The

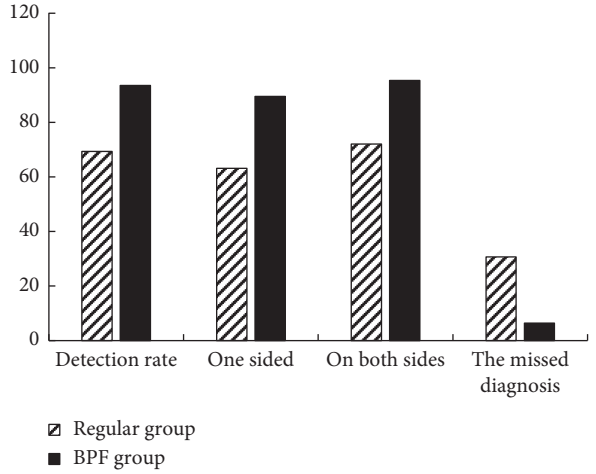

Figure 11: Comparison of the detection rate, unilateral, bilateral, and missed diagnosis rates of hypostatic pneumonia between the two groups.

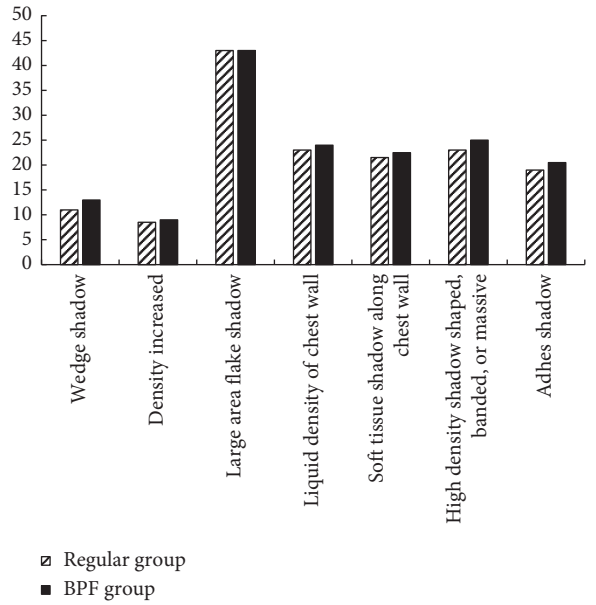

Figure 12: Comparison of the physiological characteristics of the two groups of hypostatic pneumonia.

limitations of this work are that BPF algorithm is not applied to pelvic fracture and MRI and X-ray images, and the number of patients included in this paper is not large enough, so it is hoped that BPF algorithm can be applied to the diagnosis of other diseases.

5. Conclusion

The results showed that the BPF-based CT images in the diagnosis and treatment of pelvic fractures and postoperative respiratory infections had better visual effect and better visual effect compared with the conventional CT optimization. The edge details of the image were well maintained. PSNR was better than normal optimization, and high resolution was presented, which proved that it had a high detection rate for the pendant pneumonia and was of guiding significance for the diagnosis and treatment of the disease.

Data Availability

The data used to support the findings of this study are available from the corresponding author upon request.

Conflicts of Interest

The authors declare no conflicts of interest.

References

[1] Y. Sun, H. Gu, X. Yang et al., "Bleomycin polidocanol foam (BPF) stability - in vitro evidence for the effectiveness of a novel sclerosant for venous malformations," *European*

Journal of Vascular and Endovascular Surgery, vol. 59, no. 6, pp. 1011–1018, 2020.

[2] S. B. Hallakou, G. Vial, M. Kergoat et al., "Mechanism of action of Imeglimin: a novel therapeutic agent for type 2 diabetes," *Diabetes, Obesity and Metabolism*, vol. 23, no. 3, pp. 664–673, 2021.

[3] S. Basak, M. K. Das, and A. K. Duttaroy, "Plastics derived endocrine-disrupting compounds and their effects on early development," *Birth Defects Research*, vol. 112, no. 17, pp. 1308–1325, 2020.

[4] K. Shirane, F. Miura, T. Ito, and M. C. Lorincz, "NSD1-deposited H3K36me2 directs de novo methylation in the mouse male germline and counteracts Polycomb-associated silencing," *Nature Genetics*, vol. 52, no. 10, pp. 1088–1098, 2020.

[5] I. V. Vahia, D. G. Blazer, G. S. Smith et al., "COVID-19, mental health and aging: a need for new knowledge to bridge science and service," *American Journal of Geriatric Psychiatry*, vol. 28, no. 7, pp. 695–697, 2020.

[6] Z. H. Lv and W. Q. Xiu, "Interaction of edge-cloud computing based on SDN and NFV for next generation IoT," *IEEE Internet of Things Journal*, vol. 7, no. 7, pp. 5706–5712, 2019.

[7] Y. Li and L. Xia, "Coronavirus disease 2019 (COVID-19): role of chest CT in diagnosis and management," *American Journal of Roentgenology*, vol. 214, no. 6, pp. 1280–1286, 2020.

[8] N. Tzoumas, T. E. Farrah, N. Dhaun, and D. J. Webb, "Established and emerging therapeutic uses of PDE type 5 inhibitors in cardiovascular disease," *British Journal of Pharmacology*, vol. 177, no. 24, pp. 5467–5488, 2020.

[9] Z. Ridha, L. Ouchene, E. Netchiporouk, and M. J. Gooderham, "Topical PDE-4 inhibitors are emerging for psoriasis treatment," *Journal of Cutaneous Medicine and Surgery*, vol. 25, no. 1, pp. 109-110, 2021.

[10] J. Kuhle, T. Plavina, C. Barro et al., "Neurofilament light levels are associated with long-term outcomes in multiple sclerosis," *Multiple Sclerosis Journal*, vol. 26, no. 13, pp. 1691–1699, 2020.

[11] C. E. Mordaunt, J. M. Jianu, B. I. Laufer et al., "Cord blood DNA methylome in newborns later diagnosed with autism spectrum disorder reflects early dysregulation of neurodevelopmental and X-linked genes," *Genome Medicine*, vol. 12, no. 1, p. 88, 2020.

[12] K. E. W. Suarez, A. Herold, D. Gervais et al., "Hybrid imaging of the abdomen and pelvis," *Radiologe, Der*, vol. 60, no. S1, pp. 80–89, 2020, English.

[13] J. V. Thomas, A. M. Abou Elkassem, B. Ganeshan, and A. D. Smith, "MR imaging texture analysis in the abdomen and pelvis," *Magnetic Resonance Imaging Clinics of North America*, vol. 28, no. 3, pp. 447–456, 2020.

[14] E. B. Lovsin, T. Pfister, C. Fux, D. Röthlisberger, D. Jere, and H. C. Mahler, "Use of the permitted daily exposure (PDE) concept for contaminants of intravitreal (IVT) drugs in multipurpose manufacturing facilities," *Regulatory Toxicology and Pharmacology*, vol. 101, pp. 29–34, 2019.

[15] Y. Liao, X. Li, T. Mou et al., "Distinct infection process of SARS-CoV-2 in human bronchial epithelial cell lines," *Journal of Medical Virology*, vol. 92, no. 11, pp. 2830–2838, 2020.

[16] J. L. C. Lopez, M. Miravitlles, D. L. R. Carrillo, R. Cantón, J. J. S. Cataluña, and M. A. G. Martinez, "Current challenges in chronic bronchial infection in patients with chronic obstructive pulmonary disease," *Journal of Clinical Medicine*, vol. 9, no. 6, 2020.

[17] J. Uy, J. Hawks, and C. VanSickle, "Sexual dimorphism of the relationship between the gut and pelvis in humans," *American Journal of Physical Anthropology*, vol. 173, no. 1, pp. 130–140, 2020.

[18] A. Valipour, S. B. Fernandez, A. J. Ing et al., "Bronchial rheoplasty for treatment of chronic bronchitis. Twelve-month results from a multicenter clinical trial," *American Journal of Respiratory and Critical Care Medicine*, vol. 202, no. 5, pp. 681–689, 2020.

[19] W. Y. Chan, S. Hartono, C. H. Thng, and D.-M. Koh, "New advances in magnetic resonance techniques in abdomen and pelvis," *Magnetic Resonance Imaging Clinics of North America*, vol. 28, no. 3, pp. 433–445, 2020.

[20] J. Warner, S. Desoky, H. A. Tiwari, F. Morello, D. Gilbertson, and U. Udayasankar, "Unenhanced MRI of the abdomen and pelvis in the comprehensive evaluation of acute atraumatic abdominal pain in children," *American Journal of Roentgenology*, vol. 215, no. 5, pp. 1218–1228, 2020.